Fluorescent molecular tomographic image reconstruction based on the Green's function

Wei Zou,[1,3] Jiajun Wang,[1,2,3,*] and David Dagan Feng[2,3]

[1]*School of Electronics and Information Engineering, Soochow University, Suzhou, Jiangsu, China 215021*
[2]*School of Information Technologies, University of Sydney, Sydney, Australia 2006,*
[3]*Department of Electronic and Information Engineering, Hong Kong Polytechnic University, Hong Kong*
Corresponding author: jjwang@suda.edu.cn

The rapid and accurate computation of the Jacobian matrix, which is usually computationally intensive, is of critical importance for the reconstruction problem of fluorescent molecular tomography (FMT). An extension of the Green's function method for the Jacobian matrix computation suitable for two coupled differential equations is proposed, in combination with the parallel forward computing strategy for FMT image reconstruction. For further acceleration of the reconstruction process without significant quality reduction of the results, we also propose to reconstruct the FMT image on an adaptively refined mesh generated with *a priori* information incorporated. Experimental results demonstrate that the speed of the reconstruction process can be significantly improved with the proposed overall algorithm. © 2007 Optical Society of America

OCIS codes: 170.3010, 170.3880, 170.6960, 200.4960, 260.2510.

1. INTRODUCTION

Optical techniques in the near-infrared (NIR) spectral window have made significant progress in biomedical research in recent years. The relatively low absorption and low scattering in the $600-1000$ nm spectral region allow detection of photons that have traveled through several centimeters of biological tissue [1]. Fluorescent molecular tomography (FMT) is an emerging tool for molecularly based medical imaging [2]. In this imaging modality, a fluorescent biochemical marker used as contrast agent such as Indocyanine Green is injected into the biological system. The injected fluorophore may preferentially accumulate in diseased tissues due to leaky vasculature, angiogenesis, and hypermetabolism. The use of an exogeneous fluorescent agent has the potential to improve the contrast and thus to facilitate early diagnosis [3]. During the imaging process, NIR light (sinusoidally modulated, continuous wave, or pulsed excitation light) is used to irradiate the surface of the tissue, while measurements of light that has escaped from the tissue are collected at the tissue surface, through which the spatial-concentration distribution of the fluorescence markers inside the tissue can be obtained [4]. Such distributions of fluorescent dyes have important applications in clinical diagnosis. The principle of FMT is schematically illustrated in Fig. 1.

Two processes are involved in FMT reconstruction: the forward and the inverse processes. The forward problem is to predict the observable states (e.g., emission fluence) at the measurement locations on the basis of the known excitation light source, the spatially distributed optical properties of the tissue, and the photon transport model [5]. In FMT, such a forward model is usually described by two coupled partial differential equations (i.e., diffusion equations). The first equation describes the excitation

light, while the second one corresponds to the emitted light. In the inverse problem, the values of the optical parameters (i.e., absorption coefficients and scattering coefficients), the fluorescent yield, and the fluorescent lifetime are updated repeatedly from an initial guess until the predictions match the measurements, or some other convergence criterion is achieved. The final spatial distribution of optical parameters, the fluorescent yield, and the fluorescent lifetime will result in reconstructed images.

As pointed out, both the forward and the inverse processes are involved in the tomographic image reconstruction; they will determine the speed of the reconstruction. For the forward problem, we propose a method to decouple the two originally coupled differential equations corresponding to the excitation and the emission light, making the forward problem suitable for parallel implementation. In contrast, during the inverse reconstruction process, the Jacobian matrix (also referred to as the sensitivity matrix), which defines the perturbation sensitivity of the forward calculated data to the image parameters, needs to be computed repeatedly. Hence, this process is another important factor determining the speed of the whole reconstruction algorithm.

The Jacobian matrix is usually computationally intensive especially for the FMT reconstruction problem, where there are two coupled diffusion equations describing the forward problem. It is well known that the Green's function method is an effective tool for accelerating the Jacobian matrix computing process. The theory of using the Green's function for the Jacobian matrix computing when only one differential equation is concerned has been well established. In this paper, such a method will be generalized in combination with the aforementioned parallel computing strategy for the FMT reconstruction problem where two coupled equations are concerned.
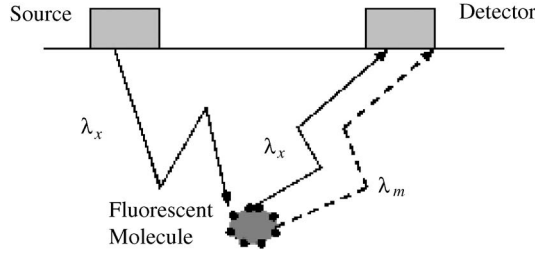
Fig. 1.   Schematic illustration of the principle of FMT.

For further acceleration of the reconstruction process without significant reduction in reconstruction quality, we also propose to reconstruct the image on an adaptively refined mesh generated with *a priori* information incorporated. Experimental results demonstrate that both the speed of the reconstruction computation and the precision of the inverse solutions can be significantly improved with the proposed algorithm. The main contribution of this paper is the combination of the proposed parallel forward computation strategy and the extension of the Green's function method originally developed for the Jacobian matrix computation from only a single differential equation to the case of two coupled equations, which can significantly speed up the reconstruction process.

2. FORWARD PROBLEM AND PARALLEL IMPLEMENTATION

A. Forward Problem
The forward model of FMT is used to predict the measurements given the locations and the optical and fluorescent properties of the random medium [5]. Light propagation is rigorously described by the Maxwell's equations that describe the relation between the electric and the magnetic waves in space and time. The radiative transfer equation (RTE) is an approximation to Maxwell's equations and has been used successfully to model light transportation in diffusive media [6]. The diffusion equation, which is the P_1 approximation to RTE, is usually employed for describing light propagation in media with either low absorption or high scattering coefficients because the RTE is extremely computationally expensive. In FMT, two coupled second-order, elliptic, partial differential equations are used to describe, respectively, the propagation of the excitation and the fluorescent light in tissues [5]. In the frequency domain, they can be written as follows:

$$(-\nabla \cdot D_x \nabla + k_x)\Phi_x = S_x,$$ (1)

$$(-\nabla \cdot D_m \nabla + k_m)\Phi_m = \beta\Phi_x.$$ (2)

The first equation describes the propagation of the excitation light, and the second one models the generation and propagation of fluorescent emitted light. In Eqs. (1) and (2), ∇ is the gradient operator, $S_x(\mathrm{W/cm^3})$ is the intensity of the excitation light source, and $\Phi_{x,m}$ is the photon fluence at the excitation (with the subscript of x) or the emission wavelength (with the subscript of m). The diffusion coefficients $D_{x,m}$, decay coefficients $k_{x,m}$, and emission source coefficients β are defined, respectively, as

$$D_x = \frac{1}{3(\mu_{axi} + \mu_{axf} + \mu'_{sx})},$$

$$D_m = \frac{1}{3(\mu_{ami} + \mu_{amf} + \mu'_{sm})},$$ (3)

$$k_x = \frac{i\omega}{c} + \mu_{axi} + \mu_{axf},$$

$$k_m = \frac{i\omega}{c} + \mu_{ami} + \mu_{amf},$$ (4)

$$\beta = \frac{\eta\mu_{axf}}{1 - i\omega\tau},$$ (5)

where $\mu_{axi}(\mathrm{cm^{-1}})$ and $\mu_{ami}(\mathrm{cm^{-1}})$ are the absorption coefficients due to nonfluorescing chromophores, $\mu_{axf}(\mathrm{cm^{-1}})$ and $\mu_{amf}(\mathrm{cm^{-1}})$ are the absorption coefficients due to the fluorophores, $\mu'_{sx}(\mathrm{cm^{-1}})$ and $\mu'_{sm}(\mathrm{cm^{-1}})$ are the isotropic scattering coefficients, η is the fluorescence quantum efficiency, $\tau(\mathrm{s})$ is the fluorescence lifetime, $i=(-1)^{1/2}$, and $c(\mathrm{cm/s})$ is the speed of light in the medium [5]. As mentioned before, the subscripts x and m are used to denote the corresponding quantities at the excitation and emission wavelengths, respectively.

To obtain solutions to Eqs. (1) and (2), the Robin-type boundary conditions are employed to describe the transport behavior of light on the boundary of the tissue:

$$\mathbf{n} \cdot [D_x \nabla \Phi_x(r)] + b_x\Phi_x(r) = 0 \qquad \text{for all } r \in \partial\Omega,$$ (6)

$$\mathbf{n} \cdot [D_m \nabla \Phi_m(r)] + b_m\Phi_m(r) = 0 \qquad \text{for all } r \in \partial\Omega,$$ (7)

where $\mathbf{n}$ is a vector normal to the boundary $\partial\Omega$, and b_x and b_m are the Robin boundary coefficients, which are governed by the reflection coefficients (R_x, R_m) [5] and have a value of $1/2$ under the condition of no reflections at the boundary.

B. Parallel Computation of the Forward Problem
The rapid and accurate computational implementation of the forward model is of critical importance for optical tomographic image reconstruction, as the forward Eqs. (1) and (2) must be solved repeatedly during the process of reconstruction following the model-based iterative image reconstruction scheme [7].

Traditionally, the forward problem of Eqs. (1) and (2) is solved in a sequential manner, i.e., Eq. (1) is first solved, and its solution is then substituted into Eq. (2), which yields the photon fluence at the emission wavelength. This sequence will prevent a fast implementation of the forward problem, and hence slow down the tomographic image reconstruction. To tackle this problem, a parallel algorithm is proposed in this paper.

To decouple Eqs. (1) and (2), the term Φ_x in the right-hand side of Eq. (2) should be eliminated. For such a purpose, a new quantity Φ is introduced that satisfies

$$(-\nabla \cdot D_m \nabla + k_m)\Phi = 1.$$ (8)

Multiplying by $\beta\Phi_x$ on both sides of Eq. (8), we can obtain

$$(-\nabla \cdot D_m \nabla + k_m)\Phi \cdot \beta\Phi_x = \beta\Phi_x. \tag{9}$$

Comparing Eqs. (2) and (9), it can be seen that Φ_m is a function of Φ and Φ_x, and hence we have

$$\Phi_m = f(\Phi, \Phi_x). \tag{10}$$

This implies that, if the function in Eq. (10) is known, the photon fluence Φ_x and Φ_m for the excitation and the emission light, respectively, can be obtained in parallel manner from Eqs. (1) and (8) with multiprocessors because Eqs. (1) and (8) are independent. Thus the whole parallel forward problem of FMT can be described by Eqs. (1) and (8) together and the photon fluence at the emission wavelength can be easily obtained by substituting the solutions to Eqs. (1) and (8) into Eq. (10). As will be seen in the following discussion, Eq. (10) can be easily solved in matrix notation when using the finite element method (FEM) for numerical implementation of the forward problem.

In the FEM, the domain is divided into P elements joined at N vertex nodes. The solution $\Phi_{x,m}$ is approximated by the piecewise function $\Phi_{x,m} = \Sigma_i^N \Phi_{xi,mi}\varphi_i$, where $\varphi_i (i=1\ldots N)$ are basis functions [8]. Assuming $V_0^h = \mathrm{span}\{\varphi_j\}_{j=1}^N$ [9], $\forall v_h \in V_0^h$, we have

$$v_h = \sum_{k=1}^N c_k \varphi_k. \tag{11}$$

Now let $u_h = \Sigma_{j=1}^N \Phi_j \varphi_j$. To obtain the weak solutions of Eqs. (1) and (2) under the boundary conditions of Eqs. (6) and (7), Eqs. (1) and (2) are written in the form

$$a_{\Omega_h}(u_h, v_h)_{x,m} = (f_{x,m}, v_h)_{\Omega_h}, \tag{12}$$

where

$$a_{\Omega_h}(u_h, v_h)_{x,m} = \int\int_{\Omega_h} [D_{x,m}(\nabla u_h \cdot \nabla v_h) + k_{x,m}u_h v_h]\mathrm{d}\Omega$$

$$+ \int_{\Gamma_h} b_{x,m}u_h v_h \mathrm{d}s, \tag{13}$$

$$(f_{x,m}, v_h)_{\Omega_h} = \int\int_{\Omega_h} f_{x,m} v_h \mathrm{d}\Omega, \tag{14}$$

$$f_x = S_x, \qquad f_m = \beta\Phi_x; \tag{15}$$

with Ω_h and Γ_h being, respectively, the bounded domain and its boundary. Equation (12) can be further rewritten in a more compact matrix form as

$$\mathbf{A}_{x,m}\mathbf{\Phi}_{x,m} = \mathbf{S}_{x,m}, \tag{16}$$

where

$$\mathbf{S}_{x,m} = \begin{bmatrix} (f_{x,m}, \varphi_1)_{\Omega_h} \\ \vdots \\ (f_{x,m}, \varphi_N)_{\Omega_h} \end{bmatrix}, \tag{17}$$

$$\mathbf{A}_{x,m} = \begin{bmatrix} a_{\Omega_h}(\varphi_1, \varphi_1)_{x,m} & \cdots & a_{\Omega_h}(\varphi_N, \varphi_1)_{x,m} \\ \vdots & & \vdots \\ a_{\Omega_h}(\varphi_1, \varphi_N)_{x,m} & \cdots & a_{\Omega_h}(\varphi_N, \varphi_N)_{x,m} \end{bmatrix}. \tag{18}$$

The elements of the finite element matrix $\mathbf{A}_{x,m}$ can be obtained from the formula

$$a_{\Omega_h}(\varphi_i, \varphi_j)_{x,m} = \int\int_{\Omega_h} D_{x,m}\nabla\varphi_i \cdot \nabla\varphi_j \mathrm{d}\Omega + \int\int_{\Omega_h} k_{x,m}\varphi_i\varphi_j \mathrm{d}\Omega$$

$$+ \int_{\Gamma_h} b_{x,m}\varphi_i\varphi_j \mathrm{d}s. \tag{19}$$

Because there are three terms in the right-hand side of Eq. (19), Eq. (16) can be rewritten as

$$(\mathbf{D}_x + \mathbf{K}_x + \mathbf{B}_x)\mathbf{\Phi}_x = \mathbf{S}_x, \tag{20}$$

$$(\mathbf{D}_m + \mathbf{K}_m + \mathbf{B}_m)\mathbf{\Phi}_m = \mathbf{S}_m, \tag{21}$$

where

$$\mathbf{A}_{x,m} = (\mathbf{D}_{x,m} + \mathbf{K}_{x,m} + \mathbf{B}_{x,m}), \tag{22}$$

$$D_{ij} = \int\int_{\Omega_h} D_{x,m}\nabla\varphi_i \cdot \nabla\varphi_j \mathrm{d}\Omega, \tag{23}$$

$$K_{ij} = \int\int_{\Omega_h} k_{x,m}\varphi_i\varphi_j \mathrm{d}\Omega, \tag{24}$$

$$B_{ij} = \int_{\Gamma_h} b_{x,m}\varphi_i\varphi_j \mathrm{d}s. \tag{25}$$

It can be proved (in Appendix A) that matrix $\mathbf{A}_{x,m}$ is symmetric and positive definite. Therefore, there exists an inverse matrix $\mathbf{H}$ for $\mathbf{A}_m$; that is, there exists a matrix $\mathbf{H}$ satisfying the following equation [10],

$$\mathbf{A}_m\mathbf{H} = \mathbf{I}, \tag{26}$$

with $\mathbf{I}$ being an identity matrix.

Combining Eqs. (20) and (26) leads to a system of equations in discretized domain for the forward problem of FMT. Owing to their independence, these two equations can be implemented in a parallel manner with multiprocessors.

It can be easily seen from Eqs. (21) and (26) that the photon fluence $\mathbf{\Phi}_m$ at the emission wavelength can be recovered by simple matrix multiplication, i.e.,

$$\mathbf{\Phi}_m = \mathbf{H} \cdot \mathbf{S}_m. \tag{27}$$

3. RECONSTRUCTION

A. Image Reconstruction

The inverse problem of FMT is to predict the spatial distribution of the optical parameters and the fluorescent properties of the medium from measurements [11]. We implement the iterative image reconstruction based on the parallel model. The Newton–Raphson technique combined with a Marquardt algorithm is employed to recon-

struct the fluorescent properties within the medium. The linearized inverse problem can be expressed as

$$\Delta \mathbf{x} = \mathbf{J}^T (\mathbf{J}\mathbf{J}^T + \lambda \mathbf{I})^{-1} \Delta \mathbf{y}, \tag{28}$$

where $\Delta \mathbf{x}$ is the perturbation in optical properties, $\Delta \mathbf{y}$ is residual data between the measurements and the predicted data, $\mathbf{J}$ is the Jacobian matrix, $\mathbf{I}$ is the identity matrix, and λ is a regularization parameter which can be derived from the Marquardt algorithm [6].

During the iterative process of Eq. (28) for FMT, the residual data of $\Delta \mathbf{y}$ are updated in each iteration with the recent distribution of $\Delta \mathbf{x}$ and, as a result, the photon fluence Φ_x and Φ_m at the excitation and emission wavelengths must be calculated repeatedly. According to Eqs. (15) and (17), $\mathbf{S}_m$ is a function of Φ_x, and hence a straightforward strategy is first to solve Eq. (20) for Φ_x, which is then substituted into Eq. (21) to obtain Φ_m. Compared with the traditional method in which Φ_x and Φ_m are obtained in a sequential manner by solving the two coupled matrix Eqs. (20) and (21) during each iteration, our parallel forward implementation scheme can compute the vector Φ_x and the matrix $\mathbf{H}$ in a parallel manner with multiprocessors from Eqs. (20) and (26) because of their independence. As a result, Φ_m can be obtained from Eq. (27) with $\mathbf{S}_m$ being obtained from Eqs. (15) and (17). Because Φ_x and the matrix $\mathbf{H}$ can be obtained simultaneously in a parallel manner and also because all operations involved in the latter process for obtaining the quantity of Φ_m are only simple matrix multiplications, this strategy can significantly speed up the reconstruction process. Particularly in the case when only the absorption coefficient μ_{axf} due to the fluorophore is to be reconstructed, the matrix $\mathbf{H}$ in Eq. (26) needs to be calculated only once during the whole reconstruction process, and the fluence Φ_m at the emission wavelength can be obtained very fast through simple matrix multiplications.

B. Jacobian Matrix Computation with the Green's Function
Another quantity that needs to be repeatedly updated during each iteration is the Jacobian matrix $\mathbf{J}$ in Eq. (28), which is also a key factor determining the implementation speed of the reconstruction algorithm. In fact, the Jacobian matrix is a measure of the rate of change in measurement with respect to the optical parameters. Conventionally, the direct derivation method and the perturbation method are two straightforward methods to obtain the Jacobian matrix, both of which are computing intensive. Therefore, it is of critical importance to develop an effective Jacobian matrix calculation method for a fast implementation of the FMT reconstruction.

The Green's function, which is also referred to as the point source function representing the field generated by a point source, plays an important role in solving both mathematical and physical problems described by partial differential equations. The theory of using the Green's function in the derivation of the Jacobian matrix from a single differential equation has been well established [12]. However, a direct employment of the aforementioned Green's function method is not valid for our case because there are two coupled forward differential equations in the FMT problem.

To solve such a problem, we propose a Green's function method based on our parallel computation algorithm as discussed in Section 2 to derive the elements of the Jacobian matrix. We will discuss in detail the derivation of the Jacobian matrix elements with respect to μ_{axf} as an example; other elements can be obtained in a similar manner.

In the framework of the FEM, we consider the following perturbations:

$$\mathbf{K}_x \to \mathbf{K}_x + \Delta \mathbf{K}_x, \qquad \mathbf{D}_x \to \mathbf{D}_x + \Delta \mathbf{D}_x, \qquad \Phi_x \to \Phi_x + \Delta \Phi_x.$$

Substituting the perturbed quantities into Eq. (20) and keeping only up to the first-order terms, we can obtain

$$\mathbf{A}_x \Delta \Phi_x = -(\Delta \mathbf{D}_x + \Delta \mathbf{K}_x)\Phi_x. \tag{29}$$

Using the Green's function as well as the corresponding reciprocity principle [13], we can get

$$(\Delta \Phi_x)_n = (\mathbf{G}_n^*)^T (\Delta \mathbf{D}_x + \Delta \mathbf{K}_x)\Phi_x, \tag{30}$$

where $\mathbf{G}_n^*$ can be obtained from the adjoint problem [14]

$$\mathbf{A}_x^* \mathbf{G}_n^* = -\mathbf{Q}_n^*, \tag{31}$$

with $\mathbf{Q}_n^*$ and $\mathbf{A}_x^*$ being, respectively, the adjoint source located at the original detector position and the conjugate matrix of $\mathbf{A}_x$.

As we are now interested only in μ_{axf}, only the perturbation corresponding to μ_{axf} should be considered with other parameters being regarded as constants. To solve the problem in the FEM framework, the perturbation of μ_{axf} at a node p $(p = 1, 2, \ldots, N)$ should be expanded in the space of V_0^h, i.e., $\Delta \mu_{axf} = \Sigma_{n=0}^N (\Delta \mu_{axf})_n \varphi_n$, with one vertex node p having a perturbation of $(\Delta \mu_{axf})_p$ and the others having a value of 0.

Dividing by $(\Delta \mu_{axf})_p$ on both sides of Eq. (30) and considering the our interest as stated in the first sentence of the last paragraph, the expression for the Jacobian matrix elements corresponding to Φ_x and μ_{axf} can be expressed as

$$J_{\mu_{axf}, \Phi_s, n, p} = \frac{(\Delta \Phi_x)_n}{(\Delta \mu_{axf})_p} = (\mathbf{G}_n^*)^T \mathbf{V}_{xp} \Phi_x, \tag{32}$$

where the elements of $\mathbf{V}_{xp}$ can be obtained from the formula:

$$(V_{xp})_{ij} = \int \int_{\Omega_k} \varphi_p \varphi_i \varphi_j \mathrm{d}\Omega. \tag{33}$$

After the derivation of the Jacobian matrix elements for Φ_x and μ_{axf} as discussed above, the next task for us is to derive the Jacobian matrix elements for Φ_m and μ_{axf}. However, owing to the coupling of the two forward Eqs. (20) and (21), Φ_m cannot be obtained from Eq. (21) separately. As a result, the Jacobian matrix elements corresponding to Φ_m and μ_{axf} cannot be derived from Eq. (21) in the same manner as those corresponding to Φ_x and μ_{axf} with the Green's function method. To tackle this problem, we propose to use the uncoupled Eqs. (20) and (26) in combination with Eq. (27) instead. Considering only a perturbation on μ_{axf} and leaving all other optical parameters unchanged, such a perturbation will have no effect on Eq. (26) and hence results in a constant matrix $\mathbf{H}$.

Then we can shift our attention to Eq. (27), and perturbations of Φ_m and $\mathbf{S}_m$ are performed as follows:

$$\Phi_m \to \Phi_m + \Delta\Phi_m, \qquad \mathbf{S}_m \to \mathbf{S}_m + \Delta\mathbf{S}_m.$$

Substituting them into Eq. (27) and neglecting the second-order terms resulting from $\Delta\mu_{axf}$ and $\Delta\Phi_x$ in $\Delta\mathbf{S}_m$, we have, according to Eqs. (2) and (5),

$$\Delta\Phi_m = \mathbf{H}\Delta\mathbf{Q}_m, \tag{34}$$

where the elements of $\Delta\mathbf{Q}_m$ can be obtained from the following formula:

$$
\begin{aligned}
(\Delta Q_m)_i &= \int\!\!\int_{\Omega_h} \frac{\eta}{1 - i\omega\tau}\Delta\mu_{axf}\Phi_x\varphi_i \mathrm{d}\Omega \\
&\quad + \int\!\!\int_{\Omega_h} \frac{\eta}{1 - i\omega\tau}\mu_{axf}\Delta\Phi_x\varphi_i \mathrm{d}\Omega \\
&= (\Delta\mu_{axf})_p \int\!\!\int_{\Omega_h} \frac{\eta}{1 - i\omega\tau}\varphi_p\Phi_x\varphi_i \mathrm{d}\Omega \\
&\quad + \int\!\!\int_{\Omega_h} \frac{\eta}{1 - i\omega\tau}\mu_{axf}\Delta\Phi_x\varphi_i \mathrm{d}\Omega.
\end{aligned}
\tag{35}
$$

Dividing both sides of Eq. (34), by $(\Delta\mu_{axf})_p$, the expression for the Jacobian matrix elements corresponding to Φ_m and μ_{axf} can be obtained as

$$\mathbf{J}_{\mu_{axf},\Phi_m,p} = \frac{\Delta\Phi_m}{(\Delta\mu_{axf})_p} = \mathbf{H}\frac{\Delta\mathbf{Q}_m}{(\Delta\mu_{axf})_p}. \tag{36}$$

Using Eq. (35), the elements of $\Delta\mathbf{Q}_m/(\Delta\mu_{axf})_p$ can be expressed as

$$
\begin{aligned}
\left[\frac{\Delta\mathbf{Q}_m}{(\Delta\mu_{axf})_p}\right]_i &= \frac{(\Delta Q_m)_i}{(\Delta\mu_{axf})_p} = \int\!\!\int_{\Omega_h} \frac{\eta}{1 - i\omega\tau}\varphi_p\Phi_x\varphi_i \mathrm{d}\Omega \\
&\quad + \int\!\!\int_{\Omega_h} \frac{\eta}{1 - i\omega\tau}\mu_{axf}\frac{\Delta\Phi_x}{(\Delta\mu_{axf})_p}\varphi_i \mathrm{d}\Omega \\
&= \int\!\!\int_{\Omega_h} \frac{\eta}{1 - i\omega\tau}\varphi_p\Phi_x\varphi_i \mathrm{d}\Omega \\
&\quad + \int\!\!\int_{\Omega_h} \frac{\eta}{1 - i\omega\tau}\mu_{axf}\sum_{n=0}^{N}\frac{(\Delta\Phi_x)_n}{(\Delta\mu_{axf})_p}\varphi_n\varphi_i \mathrm{d}\Omega.
\end{aligned}
\tag{37}
$$

Equations (32) and (36) constitute the two closed forms for the derivation of the Jacobian matrix elements with respect to μ_{axf}. From the above discussions, it can be seen that the Jacobian matrix elements corresponding to Φ_x and μ_{axf} can be calculated with the Green's function, which can then be used to calculate the Jacobian matrix elements corresponding to Φ_m and μ_{axf} based on the uncoupled equations resulting from the proposed parallel computation strategy. Therefore, the computational cost can be reduced in terms of the Green's function applied to the uncoupled equations.

Suppose the number of sources, measurements, and vertex nodes are S, M, and N, respectively. Then the direct calculation of the Jacobian matrix elements corresponding to Φ_x and μ_{axf} requires $S \times (N+1)$ FEM forward calculations, while our proposed method based on the Green's function needs only $S+M$ forward calculations. Similarly, the direct calculation of Jacobian matrix elements corresponding to Φ_m and μ_{axf} requires $S \times (N+1)$ FEM calculations while our proposed method based on the Green's function requires $S+N$ forward calculations. Therefore, when there is more than one source involved in the imaging process, our method can reduce the computation requirements and improve the reconstruction speed significantly.

C. Reconstruction Based on the Adaptively Refined Mesh

The accuracy of FEM solutions to the partial differential equations and the accuracy of the reconstructed results depend on the mesh size [15]. However, global extremely fine meshes can not only increase the complexity of the reconstruction algorithm, but also enhance the ill-posedness of the reconstruction problem because of the limited number of the measurements. To further reduce the computation requirements without significantly reducing the image resolution, we propose to reconstruct the image based on an adaptively refined mesh. During the mesh generation process, some *a priori* information derived from the structural imaging modalities can be incorporated. In our mesh generation algorithm, the reconstructed domain is first uniformly discretized according to the Delaunay triangulation scheme, after which the uniform mesh is then adaptively refined with the *a priori* information. It is obvious that in order to obtain an image with high quality, the areas with fine details should be reconstructed with high resolution, whereas other areas composed mainly of the low-frequency component with little variation can be reconstructed with low resolution to reduce the computational requirements and also to improve the ill-posedness [15].

In structural imaging, areas with large variations in pixel values, which are likely to be edges between different tissues or between normal and abnormal tissues, should be reconstructed with high resolution, whereas regions with small variations, which are likely to lie in the interior of the tissues, can be reconstructed with low resolution, which will not affect the quality of the reconstructed image. Following this idea, the variations of the pixel values in the triangle of the mesh in the structural tomography are used to judge whether the resolution is satisfied, i.e.,

$$D(X) = E\{[X - E(X)]^2\}, \tag{38}$$

where X is the pixel value in the triangular unit in the *a priori* image, E is the expectation operator, and D is the variation of pixel values in the triangle. With such a variation, adaptive meshing can be realized, in which triangles in the regions with large variations will be further segmented into finer triangles to achieve high resolution.

4. RESULTS AND DISCUSSION

To validate the algorithms proposed in this paper, they will be employed for the reconstruction of FMT from the simulated data. The simulated forward data are obtained

from Eqs. (1) and (2) in which Gaussian noise with a signal-to-noise ratio of 10 dB is added for evaluating the noise robustness of the algorithms. Figure 2 illustrates the simulated phantom with two anomalies of different shape in it. Four sources and thirty detectors corresponding, respectively, to circles and squares are equally dis-
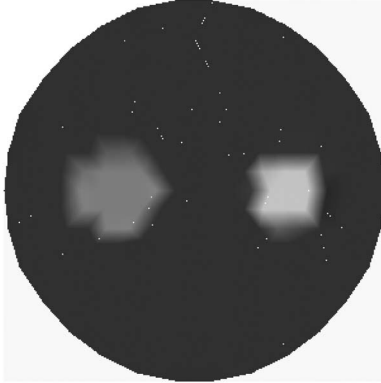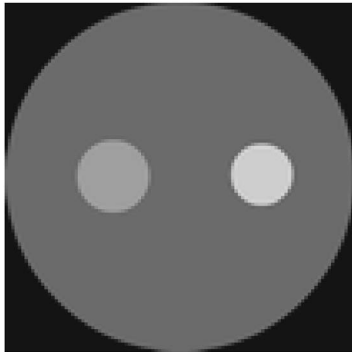

Fig. 2.   Model of reconstruction.

Fig. 3.   Model of *a priori* image.

tributed around the circumference of the simulated phantom. To achieve better reconstructed results with relatively low computational requirements, the *a priori* image with a resolution of 100×100 pixels as shown in Fig. 3 is used to generate an adaptively refined mesh. The resulting mesh is shown in Fig. 4(a) with 148 vertex nodes. Figures 4(b) and 4(c) show the globally coarse mesh with 91 vertex nodes and the globally fine mesh with 169 vertex nodes, respectively. Table 1 outlines the optical and fluorescent parameters in different regions of the simulated phantom.

To evaluate the noise robustness of our algorithm quantitatively, the relative error is introduced, defined as

$$\varepsilon_i = \frac{(x_i - x_{0i})}{x_{0i}} \times 100\,\%\,, \qquad i = 1, \ldots, M, \qquad (39)$$

where ε_i is the relative error with respect to x_i and x_{0i}, which are the reconstructed and the simulated true data, respectively, and M is the total pixel number of the original image.

The reconstruction of the absorption coefficients μ_{axf} due to the fluorophore is performed for illustration of the superiorities of parallel computation strategy. Figures 5(a) and 5(b) illustrate, respectively, the reconstructed images using the parallel computation algorithm and traditional sequential method. To further evaluate the reconstruction quality, Table 2 summarizes the performance of the reconstructions in terms of the computation time, the averaged absolute value of relative error, and the mean square error (MSE), defined as

$$\text{MSE} = \frac{1}{M} \sum_{i=1}^{M} (x_{0i} - x_i)^2. \qquad (40)$$

From Table 2, it can be seen that the reconstruction based on the parallel computation algorithm runs much
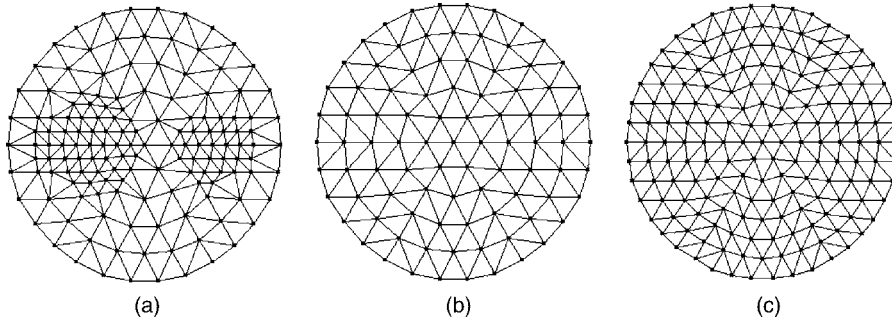

(a) (b) (c)

Fig. 4.   (a) Adaptively refined mesh, (b) globally coarse mesh, (c) globally fine mesh.

Table 1. Optical and Fluorescent Properties

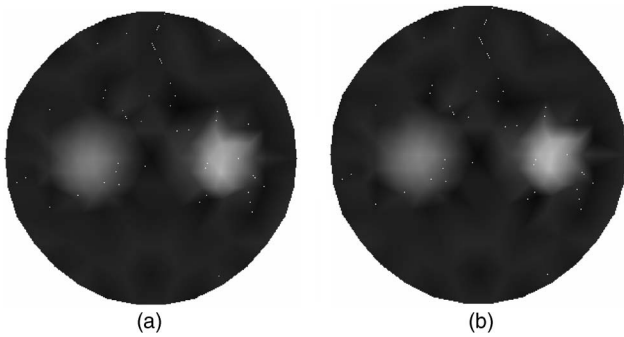|	μ_{axi} (mm)$^{-1}$	μ_{axf} (mm)$^{-1}$	μ'_{sx} (mm)$^{-1}$	η	τ (ns)
Excitation light					
Background	0.02	0.02	2.0	0.18	0.5
Heterogeneity	0.02	0.14	2.0	0.18	0.5
	μ_{ami} (mm)$^{-1}$	μ_{amf} (mm)$^{-1}$	μ'_{sm} (mm)$^{-1}$	η	τ (ns)
Fluorescent light					
Background	0.01	0.002	1.0	0.18	0.5
Heterogeneity	0.01	0.05	1.0	0.18	0.5

Fig. 5.   Reconstructed spatial map of absorption coefficient due to fluorophore μ_{axf} on the adaptively refined mesh with (a) our parallel algorithm and (b) sequential method.

Table 2. Comparison of Performance of Algorithms

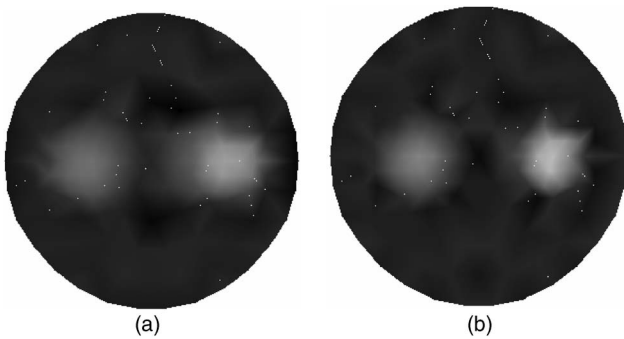| Performance	Sequential Algorithm	Parallel Algorithm
Computation time (s)	2280	1445
Mean square error	3.266×10^{-4}	3.934×10^{-4}
Averaged absolute value of relative error	2.890×10^{-2}	3.071×10^{-2}

Fig. 6.   Reconstructed spatial map of absorption coefficient due to fluorophore μ_{axf} on the adaptively refined mesh with (a) Green's function method and (b) traditional perturbation method.

Table 3. Comparison of Performance of Methods

Performance	Perturbation Method	Green's Function
Computation time (s)	1445	1034
Mean square error	3.934×10^{-4}	3.636×10^{-4}
Averaged absolute value of relative error	3.071×10^{-2}	3.011×10^{-2}

faster than the sequential method, while the MSE, as well as the averaged absolute value of the relative error of the reconstructed results based on the former, are a little larger than that based on the latter. This means that our algorithm can significantly speed up the process of reconstruction at the expense of a small reduction in reconstruction accuracy. Therefore, the parallel computation strategy can provide relatively high reconstruction quality with low computational requirements.

Figures 6(a) and 6(b) depict the reconstruction images using the Green's function method and the traditional perturbation method, respectively, both of them based on the parallel strategy. Table 3 lists the performance of the above two methods for a quantitative comparison in detail. It can be seen that the computational time of the Green's function method is less than that of the traditional perturbation method. In addition, both the MSE and the averaged absolute value of the relative error of the reconstructed results based on the former are a bit smaller than that of the latter, which means that we can further save computation time and improve the quality of reconstruction using the Green's function method. Combining Table 2 and Table 3, we can demonstrate that the Green's function method based on the parallel algorithm can significantly reduce the computational time of reconstruction with relatively high reconstruction accuracy.

To validate the advantages of the proposed reconstruction algorithm based on the adaptively refined mesh over that of the homogeneous reconstruction algorithms, reconstructed results based on the three different meshes as depicted in Figs. 4 are shown in Fig. 7, with (a), (b), and (c) corresponding, respectively, to the reconstruction result based on the adaptively refined mesh, the globally coarse mesh, and the globally fine mesh for the absorption coefficients due to fluorophores. The quantitative comparisons of the performance among the reconstructed results based on different kinds of meshes are listed in Table 4. From this table, we can see that both the MSE and the averaged absolute value of the relative error for the reconstructed tomographic image based on the adaptively refined mesh are smaller than that based on the low-resolution mesh but larger than that based on the high-resolution mesh. However, the computational requirements and the reconstruction speed of the algorithm based on the adaptively refined mesh can be significantly improved relative to that based on the uniform high-resolution mesh, i.e., we can achieve a significant compu-
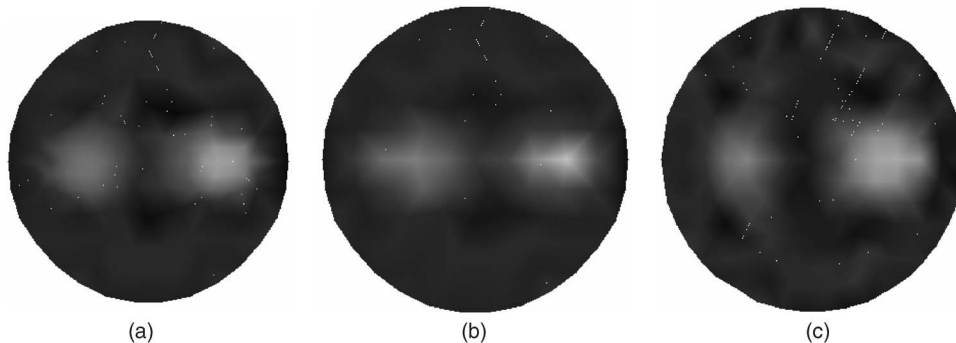

Fig. 7.   Reconstructed spatial map of absorption coefficient due to fluorophore μ_{axf} with Green's function method on (a) adaptively refined mesh, (b) globally coarse mesh, (c) globally fine mesh.

Table 4. Comparison of Reconstruction for Different Meshes

Performance	Adaptively Refined Mesh	Globally Coarse Mesh	Globally Fine Mesh
Computation time (s)	1034	178	1692
Mean square error	3.636×10^{-4}	4.679×10^{-4}	3.342×10^{-4}
Averaged absolute value of relative error	3.011×10^{-2}	3.875×10^{-2}	2.827×10^{-2}

tational reduction at a sacrifice of small reconstruction accuracy by using the reconstruction algorithm based on the adaptively refined mesh.

5. CONCLUSION

In this paper, a reconstruction algorithm suitable for multiprocessor implementation is proposed for FMT in which the traditionally computationally intensive Jacobian matrix is obtained with an algorithm combining the Green's function method and our parallel forward computation strategy. In addition, we have derived a closed form for the Jacobian matrix elements in terms of the Green's function that greatly reduces the computational complexity. For a further reduction of the computing requirements and for the improvement of the ill-posedness of the reconstruction problem, the tomographic image is proposed to be reconstructed on an adaptively refined mesh in which *a priori* information obtained from other imaging modalities can be conveniently incorporated. Experimental results show that our algorithm can significantly speed up the reconstruction process and achieve high accuracy.

APPENDIX A

(1) $\mathbf{A}_{x,m}$ is symmetric.

Proof. It can obviously be seen from Eqs. (18) and (19) that

$$a_{\Omega_h}(\varphi_i, \varphi_j)_{x,m} = a_{\Omega_h}(\varphi_j, \varphi_i)_{x,m}. \tag{A1}$$

Thus, we can conclude that

$$\mathbf{A}_{x,m}{}^T = \mathbf{A}_{x,m}. \tag{A2}$$

Therefore $\mathbf{A}_{x,m}$ is symmetric. □

(2) $\mathbf{A}_{x,m}$ is positive definite.

Proof.

Definition 1: For a matrix $\mathbf{A} \in \mathbf{C}^{N \times N}$, $\forall \mathbf{X} \in \mathbf{C}^N$, $\mathbf{X} \neq 0$, if $\mathrm{Re}(\mathbf{X}^H \mathbf{A} \mathbf{X}) > 0$, matrix $\mathbf{A}$ is a complex positive definite matrix [16].

Definition 2: For a continuous function f defined on Ω_h with boundary Γ_h, the norm of f can be defined as [9]

$$\|f\|_{1,\Omega_h} = \left\{ \int\!\!\int_{\Omega_h} [f^2 + (f'_x)^2 + (f'_y)^2] \mathrm{d}\Omega + \int_{\Gamma_h} f^2 \mathrm{d}s \right\}^{1/2}. \tag{A3}$$

Let $\mathbf{V} = (c_1, \ldots, c_N)^T \in \mathbf{C}^N$ and $\mathbf{V} \neq 0$, where $\mathbf{V}^H$ is the conjugate transposed matrix of $\mathbf{V}$, $\bar{c}$ is the conjugate complex of c, and $\mathrm{Re}(X)$ is the real part of complex X; we have

$$\mathrm{Re}(\mathbf{V}^H \mathbf{A}_{x,m} \mathbf{V}) = \mathrm{Re}\left[\sum_{i,j=1}^N a_{\Omega_h}(\varphi_i, \varphi_j)_{x,m} \bar{c}_i c_j \right]$$

$$= \mathrm{Re}\left[a_{\Omega_h}\left(\sum_{i=1}^N \bar{c}_i \varphi_i, \sum_{j=1}^N c_j \varphi_j \right)_{x,m} \right]$$

$$= \mathrm{Re}[a_{\Omega_h}(\bar{v}_h, v_h)_{x,m}], \tag{A4}$$

$$\mathrm{Re}(a_{\Omega_h}(\bar{v}_h, v_h)_{x,m})$$

$$= \mathrm{Re}\left(\int\!\!\int_{\Omega_h} \left\{ D_{x,m}\left[\left| \frac{\partial v_h}{\partial x} \right|^2 + \left| \frac{\partial v_h}{\partial y} \right|^2 \right] + k_{x,m} |v_h|^2 \right\} \mathrm{d}\Omega \right.$$

$$+ \left. \int_{\Gamma_h} b_{x,m} |v_h|^2 \mathrm{d}s \right) \geqslant \gamma_1 \left\{ \int\!\!\int_{\Omega_h} \left[\left| \frac{\partial v_h}{\partial x} \right|^2 + \left| \frac{\partial v_h}{\partial y} \right|^2 \right] \mathrm{d}\Omega \right.$$

$$+ \left. \int_{\Gamma_h} |v_h|^2 \mathrm{d}s \right\}$$

$$= \frac{1}{2} \gamma_1 \left\{ \int\!\!\int_{\Omega_h} \left[\left| \frac{\partial v_h}{\partial x} \right|^2 + \left| \frac{\partial v_h}{\partial y} \right|^2 \right] \mathrm{d}\Omega + \int_{\Gamma_h} |v_h|^2 \mathrm{d}s \right\}$$

$$+ \frac{1}{2} \gamma_1 \left\{ \int\!\!\int_{\Omega_h} \left[\left| \frac{\partial v_h}{\partial x} \right|^2 + \left| \frac{\partial v_h}{\partial y} \right|^2 \right] \mathrm{d}\Omega + \int_{\Gamma_h} |v_h|^2 \mathrm{d}s \right\}, \tag{A5}$$

where $\gamma_1 = \min[1, (b_{x,m}/D_{x,m})_{\min}] D_{x,m \ \min}$.

Let $v_h = a + bi$, $a, b \in R$; then we obtain

$$\left| \frac{\partial v_h}{\partial x} \right|^2 = \left(\frac{\partial a}{\partial x} \right)^2 + \left(\frac{\partial b}{\partial x} \right)^2 = \frac{1}{4(a^2+b^2)}\left[4a^2 \left(\frac{\partial a}{\partial x} \right)^2 \right.$$

$$+ 4b^2 \left(\frac{\partial b}{\partial x} \right)^2 + 4a^2 \left(\frac{\partial b}{\partial x} \right)^2 + \left. 4b^2 \left(\frac{\partial a}{\partial x} \right)^2 \right]$$

$$\geqslant \frac{1}{4(a^2+b^2)}\left[4a^2 \left(\frac{\partial a}{\partial x} \right)^2 + 4b^2 \left(\frac{\partial b}{\partial x} \right)^2 \right.$$

$$+ \left. 8 \left| ab \frac{\partial b}{\partial x} \cdot \frac{\partial a}{\partial x} \right| \right]$$

$$\geqslant \frac{1}{4(a^2+b^2)}\left[4a^2 \left(\frac{\partial a}{\partial x} \right)^2 + 4b^2 \left(\frac{\partial b}{\partial x} \right)^2 \right.$$

$$+ \left. 8ab \frac{\partial b}{\partial x} \cdot \frac{\partial a}{\partial x} \right], \tag{A6}$$

$$\left(\frac{\partial |v_h|}{\partial x} \right)^2 = \left(\frac{\partial \sqrt{a^2+b^2}}{\partial x} \right)^2 = \frac{1}{4(a^2+b^2)}\left[\frac{\partial(a^2)}{\partial x} + \frac{\partial(b^2)}{\partial x} \right]^2$$

$$= \frac{1}{4(a^2+b^2)}\left[2a \frac{\partial a}{\partial x} + 2b \frac{\partial b}{\partial x} \right]^2$$

$$= \frac{1}{4(a^2+b^2)}\left[4a^2 \left(\frac{\partial a}{\partial x} \right)^2 + 4b^2 \left(\frac{\partial b}{\partial x} \right)^2 \right.$$

$$+ \left. 8ab \frac{\partial b}{\partial x} \cdot \frac{\partial a}{\partial x} \right]. \tag{A7}$$

From Eqs. (A6) and (A7), we can conclude that

$$\left|\frac{\partial v_h}{\partial x}\right|^2 \geq \left(\frac{\partial |v_h|}{\partial x}\right)^2. \tag{A8}$$

Similarly, we also have

$$\left|\frac{\partial v_h}{\partial y}\right|^2 \geq \left(\frac{\partial |v_h|}{\partial y}\right)^2. \tag{A9}$$

Using Friedrich's inequality [9],

$$\int\int_{\Omega}\left[\left(\frac{\partial v}{\partial x}\right)^2 + \left(\frac{\partial v}{\partial y}\right)^2\right]\mathrm{d}\Omega + \int_{\Gamma} v^2\mathrm{d}s \geq c\int\int_{\Omega} v^2\mathrm{d}\Omega, \tag{A10}$$

with constant $c > 0$ in combination with Eqs. (A3), (A8), and (A9), we have

$$\begin{aligned}
\mathrm{Re}[a_{\Omega_h}(\bar{v}_h, v_h)_{x,m}] &\geq \frac{1}{2}\gamma_1\Bigg\{\int\int_{\Omega_h}\left[\left(\frac{\partial |v_h|}{\partial x}\right)^2 + \left(\frac{\partial |v_h|}{\partial y}\right)^2\right]\mathrm{d}\Omega \\
&\quad + \int_{\Gamma_h}|v_h|^2\mathrm{d}s\Bigg\} + \frac{1}{2}\gamma_1\Bigg\{\int\int_{\Omega_h}\Bigg[\left|\frac{\partial v_h}{\partial x}\right|^2 \\
&\quad + \left|\frac{\partial v_h}{\partial y}\right|^2\Bigg]\mathrm{d}\Omega + \int_{\Gamma_h}|v_h|^2\mathrm{d}s\Bigg\} \\
&\geq \frac{1}{2}\gamma_1 c\int\int_{\Omega_h}|v_h|^2\mathrm{d}\Omega \\
&\quad + \frac{1}{2}\gamma_1\Bigg\{\int\int_{\Omega_h}\Bigg[\left|\frac{\partial v_h}{\partial x}\right|^2 + \left|\frac{\partial v_h}{\partial y}\right|^2\Bigg]\mathrm{d}\Omega \\
&\quad + \int_{\Gamma_h}|v_h|^2\mathrm{d}s\Bigg\} \\
&= \frac{1}{2}\gamma_1\Bigg\{c\int\int_{\Omega_h}|v_h|^2\mathrm{d}\Omega + \int\int_{\Omega_h}\Bigg[\left|\frac{\partial v_h}{\partial x}\right|^2 \\
&\quad + \left|\frac{\partial v_h}{\partial y}\right|^2\Bigg]\mathrm{d}\Omega + \int_{\Gamma_h}|v_h|^2\mathrm{d}s\Bigg\} \\
&\geq \frac{1}{2}\gamma_1\Bigg\{c\int\int_{\Omega_h}|v_h|^2\mathrm{d}\Omega \\
&\quad + \int\int_{\Omega_h}\left[\left(\frac{\partial |v_h|}{\partial x}\right)^2 + \left(\frac{\partial |v_h|}{\partial y}\right)^2\right]\mathrm{d}\Omega \\
&\quad + \int_{\Gamma_h}|v_h|^2\mathrm{d}s\Bigg\} \geq \gamma\|\|v_h\|\|^2_{1,\Omega_h}, \tag{A11}
\end{aligned}$$

where $\gamma = (1/2)\gamma_1\min(1,c)$.

From Eqs. (A4) and (A11) we have

$$\mathrm{Re}(\mathbf{V}^H\mathbf{A}_{x,m}\mathbf{V}) = \mathrm{Re}[a_{\Omega_h}(\bar{v}_h, v_h)_{x,m}] \geq \gamma\|\|v_h\|\|^2_{1,\Omega_h} > 0,$$

$$\forall\, \mathbf{V} \neq 0. \tag{A12}$$

Therefore according to definition 1, matrix $\mathbf{A}_{x,m}$ is positive definite, as stated. $\qquad\square$

ACKNOWLEDGMENTS

REFERENCES

1. A. Yodh and B. Chance, "Spectroscopy and imaging with diffusing light," Phys. Today **48**, 34–40 (1995).
2. R. B. Schulz, J. Ripoll, and V. Ntziachristos, "Experimental Fluorescence Tomography of Tissues With Noncontact Measurements," IEEE Trans. Med. Imaging **23**, 492–500 (2004).
3. A. B. Milstein, S. Oh, K. J. Webb, C. A. Bouman, Q. Zhang, D. A. Boas, and R. P. Millane, "Fluorescence optical diffusion tomography," Appl. Opt. **42**, 3081–3094 (2003).
4. A. D. Klose, V. Ntziachristos, and A. H. Hielscher, "The inverse source problem based on the radiative transfer equation in optical molecular imaging," J. Comput. Phys. **202**, 323–345 (2005).
5. F. Fedele, M. J. Eppstein, J. P. Laible, A. Godavarty, and E. M. Sevick-Muraca, "Fluorescence photon migration by the boundary element method," J. Comput. Phys. **210**, 1–24 (2005).
6. A. P. Gibson, J. C. Hebden, and S. R. Arridge, "Recent advances in diffuse optical imaging," Phys. Med. Biol. **50**, R1–R43 (2005).
7. A. Y. Bluestone, M. Stewart, J. Lasker, G. S. Abdoulaev, and A. H. Hielscher, "Three-dimensional optical tomographic brain imaging in small animals, Part 1:hypercapnia," J. Biomed. Opt. **9**, 1046–1062 (2004).
8. S. R. Arridge, "Optical tomography in medical imaging," Inverse Probl. **15**, R41–R93 (1999).
9. Q. Lin, *Basic Text Book of Numerical Solution Method for Differential Equations*, 2nd ed. (Science Press, 2003).
10. J. Li, "Research on positive definiteness of matrix," Practice Cogn. Math. **2**, 59–63 (1995).
11. D. Y. Paithankar, A. U. Chen, B. W. Pogue, M. S. Patterson, and E. M. Sevick-Muraca, "Imaging of fluorescent yield and lifetime from multiply scattered light reemitted from random media," Appl. Opt. **36**, 2260–2272 (1997).
12. S. R. Arridge and M. Schweiger, "A general framework for iterative reconstruction algorithms in optical tomography using a finite element method," in *Computational Radiology and Imaging: Therapy and Diagnosis*, IMA Volumes in Mathematics and Its Applications (Springer-Verlag, 1998).
13. Z. Pan, *Text Book of Maths and Physics Methods* (Nankai University Press, 1993).
14. S. R. Arridge and J. C. Hebden, "Optical imaging in medicine: II. Modelling and reconstruction," Phys. Med. Biol. **42**, 841–853 (1997).
15. A. Joshi, W. Bangerth, and E. M. Sevick-Muraca, "Adaptive finite element based tomography for fluorescence optical imaging in tissue," Opt. Express **12**, 5402–5417 (2004).
16. X. Pang, "The research on positive definite complex matrix," J. Shandong Univ. 38, 66–69 (2003).